MODIS Reflectance and Active Fire Data for Burn Mapping in Colombia

Silvia Merino-de-Miguel*

EUIT Forestal, Technical University of Madrid, Madrid, Spain

Federico González-Alonso

Remote Sensing Laboratory, CIFOR-INIA, Madrid, Spain

Margarita Huesca

ETSI Montes, Technical University of Madrid, Madrid, Spain

Dolors Armenteras and Carol Franco

Department of Biology, National University of Colombia, Bogotá, Colombia

Received 30 March 2010; accepted 24 October 2010

ABSTRACT: Satellite-based strategies for burned area mapping may rely on two types of remotely sensed data: postfire reflectance images and active fire detection. This study uses both methods in a synergistic way. In particular, burned area mapping is carried out using MCD43B4 [Moderate Resolution Imaging Spectrometer (MODIS); *Terra* + *Aqua* nadir bidirectional reflectance distribution function (BRDF); adjusted reflectance 16-day L3 global 1-km sinusoidal grid V005 (SIN)] postfire datasets and MODIS active fire products. The developed methodology was tested in Colombia, an area not covered by any known MODIS ground antenna, using data from 2004. The resulting burned area map was validated using a high-spatial-resolution Landsat-7 Enhanced Thematic Mapper Plus (ETM+) image and compared to two global burned area

* Corresponding author address: Dr. Silvia Merino-de-Miguel, UD Topografía, EUIT Forestal (UPM), Ciudad Universitaria, Madrid 28040, Spain.
E-mail address: silvia.merino@upm.es

DOI: 10.1175/2010EI344.1

products: L3JRC (terrestrial ecosystem monitoring global burnt area product) and MCD45A1 (MODIS *Terra* + *Aqua* burned area monthly global 500-m SIN grid V005). The results showed that this method would be of great interest at regional to national scales because it proved to be quick, accurate, and cost effective.

KEYWORDS: Remote sensing; Forest fires; NBR index

1. Introduction

Wildfire is a critical Earth-system process that has significant influences on both terrestrial and atmospheric conditions, especially in relation to vegetation dynamics, biogeochemical cycling, and atmospheric chemistry. In South America, wildfires cause these conditions to change and have an impact on a number of other conditions associated not only with forest composition but also with the structure and functioning of the tropical forest (Cochrane and Laurance 2008) and the savannah ecosystem (Hoffmann et al. 2003). In 2004, most of the vegetation fires in South America occurred in Brazil, followed by Argentina, Colombia, and Bolivia (Chuvieco et al. 2008), and they were mostly driven by deforestation and agriculture (Cochrane and Laurance 2008). Annual carbon emissions derived from these wildfires vary in their estimated figures. However, South America is considered to contribute, on average, up to 13% of the world's fire carbon emissions because of vegetation burning (Van der Werf et al. 2006). In fact, vegetation fires in Colombia have become an important issue since the publication of the first studies showing the contribution of these fires to the total burn area mapping at both local and regional scales (Armenteras et al. 2005; Armenteras et al. 2009; Chuvieco et al. 2008).

As occurs in a variety of ecological applications, regional to global fire studies require data from broad spatial extents, which cannot be collected using field-based methods (Kerr and Ostrovsky 2003). Therefore, ecologists and conservation biologists are turning to remote sensing to provide the methods and data sources necessary to model these environmental changes (Kerr and Ostrovsky 2003). Information on fire activity, which is characterized using burned area maps, is used for research on global changes, estimating atmospheric emissions, and developing periodic global and regional assessments. It is also used for fire and ecosystem management planning and operational purposes, as well as the development of informed policies. For all of these reasons, the development of rapid, accurate, and reliable burned area maps—a task affordable at present only by using remote sensing data—is of particular importance.

The use of remote sensing data provides temporal and spatial coverage of biomass burning without the need for costly and intensive fieldwork. Among the available sensors, the use of *Terra*/*Aqua* Moderate Resolution Imaging Spectrometer (MODIS), Système Pour l'Observation de la Terre (SPOT) VEGETATION (VGT), or *European Remote Sensing Satellite-2* (*ERS-2*) Along Track Scanning Radiometer-2 (ATSR-2) are especially extensive. These systems have allowed several global estimates of burned areas to be produced during the last decade: GLOBSCAR (ATSR Global Burned Forest Mapping) (Simon et al. 2004), Global Burnt Area 2000 (GBA2000; Grégoire et al. 2003), L3JRC (Global VGT Burnt Area Product 2000–07) (Tansey et al. 2008), and MCD45 (MODIS burned area product) (Roy

et al. 2005; Roy et al. 2008) are some examples. Additionally, a number of other regional products have also been developed, such as the Areas Quemadas de Latinoamérica 2004 (AQL2004; Latin America burned area map for 2004) (Chuvieco et al. 2008), which estimated 153 215 km^2 of burned area for South America in 2004, 19 449 km^2 (12.7%) of which was located in Colombia. Despite these and other similar products, burned area mapping is still not a fully resolved issue because comparison among the available figures is, in some cases, challenging. Chang and Song (Chang and Song 2009) compared two global burned area products for the period 2000–06: L3JRC (Tansey et al. 2008) and MCD45 (Roy et al. 2005). At a global scale, the resulting mean for the annual burned area was 4 010 858 or 3 465 434 km^2, according to L3JRC and MCD45, respectively. In the case of South America, the mean annual figure was 360 882 km^2 (representing 9% of the global burned area and 2% of the continental area) or 176 601 km^2 (5% of global burned area; 1% of the continental area) according to L3JRC and MCD45, respectively (Chang and Song 2009). These and other results point to the need for more validation and, more generally, to the advantage of combining a series of satellite-derived fire products to get the benefits of their respective strengths (Boschetti et al. 2004a).

Satellite-based strategies for burn mapping may rely on two types of remote sensing data: postfire reflectance images and active fires, both of which may be used separately or in combination (Fraser et al. 2000). Among the different methods for burn mapping by means of reflectance postfire satellite data, the use of spectral indices is one of the most widespread. Vegetation indices [e.g., normalized difference vegetation index (NDVI)], for which estimation typically involves data from the red and near-infrared (NIR) bands, have been commonly used to derive vegetation properties but also to discriminate and map burned areas. As shown by Lentile et al. (Lentile et al. 2006), in most environments and fire regimes and at the spatial resolution of most satellite sensors (>30 m), burned vegetation results in a drastic reduction in NIR surface reflectance; this is typically accompanied by a rise in shortwave-infrared (SWIR) reflectance. Thus, several spectral indices have been created to integrate the NIR and SWIR bands, both of which register the strongest responses, in opposite ways, to burning (Roldán-Zamarrón et al. 2006). This is the case for the normalized burn ratio (NBR) and the differenced NBR (dNBR) developed by Key and Benson (Key and Benson 1999), which have been used for burn mapping at regional to global scales by Loboda et al. (Loboda et al. 2007), among others.

In addition to the use of spectral indices, several studies have shown the utility of active fire detection for burn mapping. In active fire detection, fire thermal energy, as measured by midinfrared channels, is used to identify active fires. In a second step, scar mapping is developed: based, for example, on the total number of active fires (Pozo et al. 1997). However, it is difficult to relate active fires to actual burned area because the satellite may not pass over at the time of the fire, or the fire may be obscured because of cloud cover or dense smoke (Roy et al. 2002). Other difficulties for burn mapping using active fires may be due to variability in fuel conditions or differences in fire behavior (Giglio et al. 2006b). These issues can be solved through the combination of collecting active fire information together with spectral indices. Following this model, Roy et al. (Roy et al. 1999) developed a multitemporal burn scar detection algorithm that used a time series of burn scar index

data (based on a vegetation index) derived from Advanced Very High Resolution Radiometer (AVHRR) daily images to compute a burn scar index change map that was then classified using thresholds derived from the output of an active fire detection algorithm. Fraser et al. (Fraser et al. 2000) also used AVHRR data to develop their hotspot and NDVI differencing synergy (HANDS) algorithm, an approach that combines the strengths of hotspot detection and NDVI differencing for boreal burned area mapping. Al-Rawi et al. (Al-Rawi et al. 2001) tried to go beyond designing a system for monitoring the status of a fire in real time by creating a system that would also produce a near-real-time burned area map. To do so, Al-Rawi et al. (Al-Rawi et al. 2001) used NDVI maximum value composites in addition to active fire locations, both of which were derived from AVHRR data. Another approach was taken by Pu et al. (Pu et al. 2004), who proposed an algorithm based on daily dynamics of fires, which were then used to obtain information on active fires and burn scars by using AVHRR data from California for NDVI calculation and hotspot detection. More recently, Loboda et al. (Loboda et al. 2007) proposed a regionally adaptable semiautomated approach to mapping burned areas using MODIS surface reflectance 8-day composite product (MOD09A1) and MODIS active fire product (MOD14). Finally, we should mention the work published by Giglio et al. (Giglio et al. 2009), which consisted of an automated hybrid algorithm used for burn mapping via MODIS imagery and active fire observations. This method detects persistent changes in data derived from MODIS during a series of daily surveys.

This study assessed the development of a method for rapid and accurate estimation and mapping of burned areas at a regional scale. Its findings are applied in Colombia (South America) for the assessment of the 2004 fire season. The algorithm we developed integrates, in a synergistic way, a spectral index together with active fire data, both of which are derived from MODIS data, and it is based on previous methods developed and successfully tested in Spanish environments (Huesca et al. 2008; González-Alonso and Merino-de-Miguel 2009; Merino-de-Miguel et al. 2010). The resulting burned area map was validated using a high-spatial-resolution Landsat-7 Enhanced Thematic Mapper Plus (ETM+) image that partially covers the study area. Following that, the resulting 1-km-spatial-resolution MODIS-based burn map was compared to two global burned area products with similar characteristics (L3JRC and MCD45A1). Finally, because there is not much peer-reviewed literature about this topic available, this work is also an investigation into the use of nadir bidirectional reflectance distribution function (BRDF)-adjusted reflectance products.

2. Study area and data description

Our approach is applied here to Colombia (Figure 1), where hundreds if not thousands of wildfires occur every year during the dry season. Although vegetation fires are found throughout the country (Armenteras et al. 2009), the Orinoco basin savannas (so-called Los Llanos Orientales) are of great importance because of their climatic seasonality and the intensity of human pressure (Armenteras et al. 2005). In this region, most of the wildfires are human induced, mainly by farmers that use fire for slash-and-burn practices. Most burning occurs during the dry season (December–March) as a way to obtain fresh grass for cattle and to clear fields for cultivation later in the year. There is neither an official record of wildfire statistics

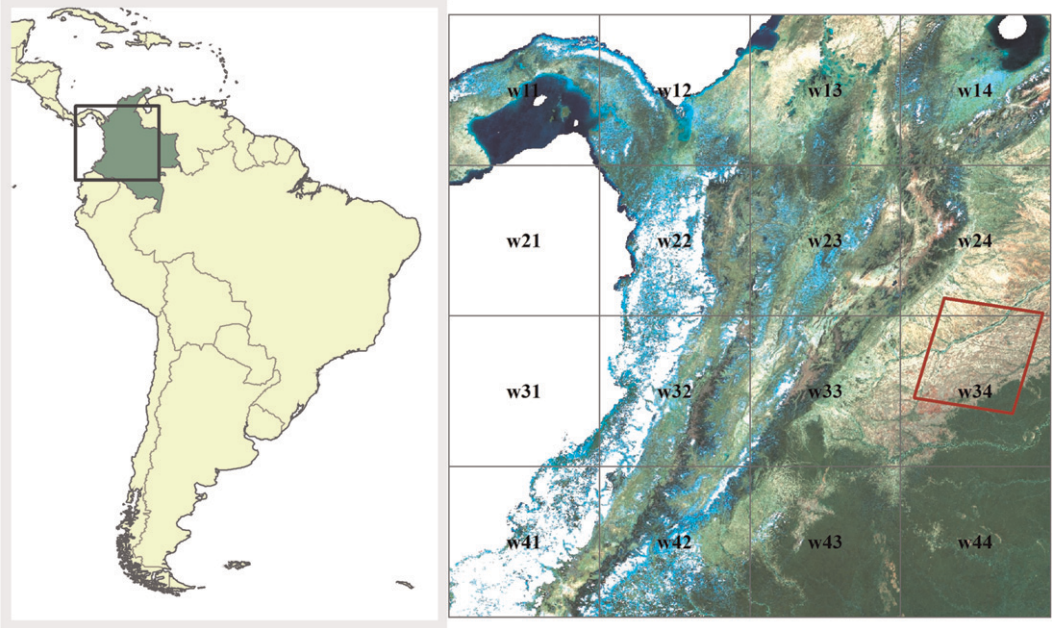

Figure 1. Study area: Colombia (in green), MODIS H10V08 tile (top-left corner is 10°N, 80°W and bottom-right corner is 0°, 70°W) and location (in red) of the validation dataset (Landsat-7 ETM+).

in Colombia nor concordant burned area figures among the available remotely sensed products. For example, according to the GLOBSCAR product, the affected area for Colombia in 2000 was 14 866 km^2 (Simon et al. 2004), whereas according to the GBA2000 it was 9692 km^2 (Tansey et al. 2004). The AQL2004 (Chuvieco et al. 2008) estimated 19 500 km^2 of burned area for Colombia in 2004, whereas Armenteras et al. (Armenteras et al. 2005) stated that 4882 km^2 were burned in Los Llanos Orientales during 2001. These results emphasize the need for more reliable and regionally adapted burned area algorithms.

In this study, three sets of data were used for burn mapping development: (i) a postfire reflectance MODIS product (MCD43B4–2004025: MODIS *Terra* + *Aqua* nadir BRDF-adjusted reflectance 16-day L3 global 1 km; 25 January–9 February 2004) (Figure 1); (ii) MODIS active fire locations (MOD14 and MYD14: MODIS *Terra* and *Aqua* thermal anomalies; 1 January–2 February 2004); and (iii) ancillary maps and information, which consisted of administrative maps for masking purposes. For validation purposes, we used a Landsat ETM+ image [Worldwide Reference System-2 (WRS-2), path 006, row 057; 1 February 2004] (NASA Landsat Program 2004]. For comparison purposes, we used two datasets: (i) L3JRC-2004 (global, daily, SPOT VGT–derived burned area product) and (ii) MCD45A1–2005001 (MODIS *Terra* + *Aqua* burned area monthly L3 global 500 m; 1–31 January 2004).

The area covered by the MODIS image that was used in this study (tile H10V08) was 1200 km by 1200 km. It was divided into 16 subimages of 300 km by 300 km (Figure 1), which were referred to as w11 through w44 for algorithm development purposes.

MODIS is a sensor on board the *Terra* and *Aqua* satellites with more than 30 channels at variable spatial resolutions (250, 500, and 1000 m). We used one postfire MODIS product that was downloaded from the Earth Observing Systems (EOS) Data Gateway free of charge, and it consisted of nadir BRDF-adjusted surface reflectance in the optical range (seven bands: visible to shortwave-infrared wavelengths) at a 1000-m spatial resolution (MCD43B4). This product is computed for each of the seven spectral bands at the mean solar zenith angle of each 16-day period, therefore removing directional effects and producing a much more radiometrically consistent image, as can be seen in Figure 1. A general description of this product can be found in Schaaf et al. (Schaaf et al. 2002). Nadir BRDF-adjusted reflectance (NBAR) products are currently being used for the production of the global MODIS land-cover product (MOD12Q1) (Friedl et al. 2000), and it is expected that the NBAR products will be used profusely for those situations where composited surface reflectance may have been traditionally used (Schaaf 2010), as occurs for burn mapping in areas of persistent cloud cover, of which Colombia is a good example.

The MODIS hotspots/active fire detections (NASA/University of Maryland 2002), as provided free of charge through the Internet, consisted of a set of shape files with one record per active fire. Information related to each active fire included: location (latitude and longitude), date, time, confidence level, and the type of satellite involved (*Terra* or *Aqua*). A general description of the MODIS fire products can be found in the paper published by Justice et al. (Justice et al. 2002), whereas a detailed description of the MODIS active fire detection algorithm can be found in the studies published by Giglio et al. (Giglio et al. 2003; Giglio et al. 2006a; Giglio et al. 2006b).

The Landsat-7 ETM+ that we used for validation was downloaded free of charge through the Internet from the Global Land Cove Facility (NASA Landsat Program 2004). Finally, the L3JRC product was downloaded from the Global Environment Monitoring Web site, and the MODIS burned area product (MCD45A1) was downloaded from the EOS Data Gateway, both of which were free of charge. A general description of the L3JRC can be found in the paper published by Tansey et al. (Tansey et al. 2008), whereas a general description of the MODIS burned area products can be found in two papers published by Roy et al. (Roy et al. 2005; Roy et al. 2008).

3. Data analysis

The burn mapping method that we proposed followed three steps: (i) NBR calculation using the MODIS nadir BRDF-adjusted reflectance product, (ii) NBR threshold establishment using the MODIS active fires, and (iii) burned area mapping. Afterward, we first validated the MODIS-based burn map using a high-spatial-resolution image and then compared it against two global burned area products (L3JRC and MCD45A1). Figure 2 summarizes all of these tasks in a flowchart. Image and data processing were carried out using ENVI 4.5 and ArcGIS 9.3 software packages.

The NBR (Key and Benson 1999) is a spectral index that integrates NIR and SWIR bands, both of which register the strongest responses, albeit in opposite

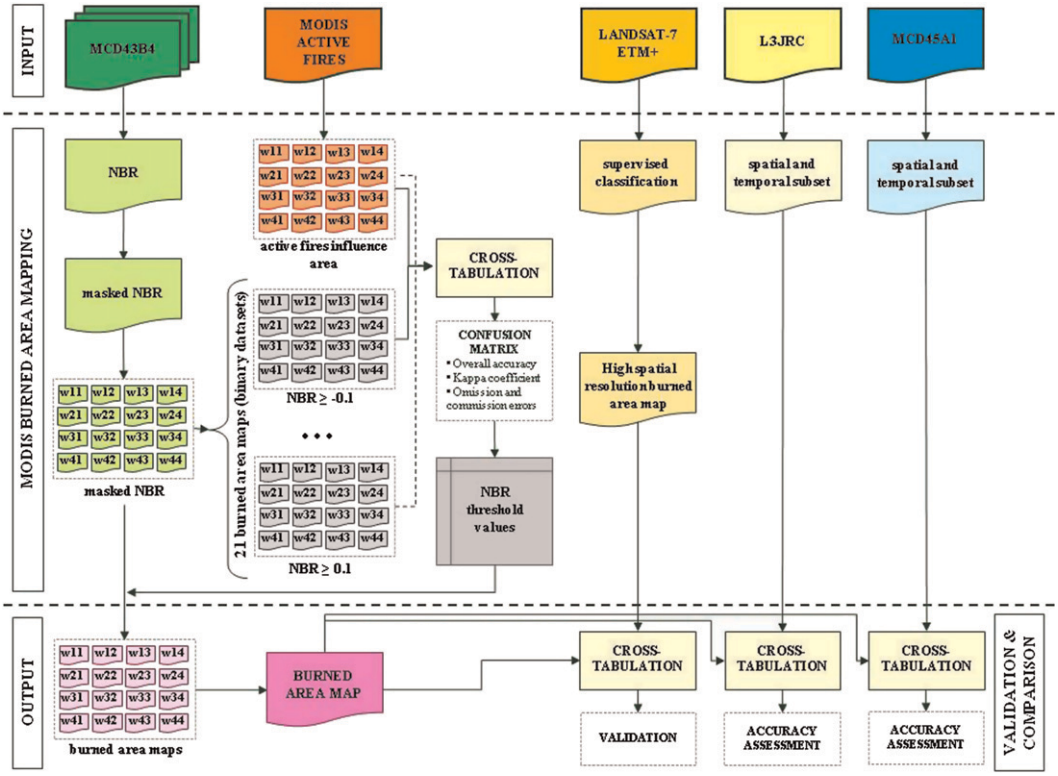

Figure 2. Methodology followed in this work.

ways, to burning (Lentile et al. 2006; Roldán-Zamarrón et al. 2006). The NBR is estimated using the following equation:

$$\mathrm{NBR} = \frac{(\rho_{\mathrm{SWIR}} - \rho_{\mathrm{NIR}})}{(\rho_{\mathrm{SWIR}} + \rho_{\mathrm{NIR}})}, \tag{1}$$

where ρ_{swir} and ρ_{nir} are the SWIR and NIR pixel reflectance values, respectively. From Equation (1), the NBR was calculated using bands 2 (NIR) and 7 (SWIR) of the MCD43B4 product. The result was masked for incoherent values (e.g., out-of-range NBR values, due to incoherent reflectance values) and no-land pixels, both of which were labeled as no-data pixels. Once the NBR image had been properly masked, a suitable threshold had to be established to distinguish between burned and unburned pixels. It is recognized that an effective threshold for separating burns is spatially variable (Fraser et al. 2000) because both the surface itself and the sensing system introduce variations in space (Roy et al. 2002). All of the studies carried out on this subject have used one of the two possible approaches of fixed or variable thresholds. Many authors have favored the use of the variable approach, but in this study we have opted for the fixed approach together with a stratification of the variable prior to threshold determination. The stratification process consisted

of dividing the study area (a 1200 km by 1200 km image) into 16 subimages of 300 km by 300 km (Figure 1). Therefore, NBR threshold establishment was done on a per subimage basis; that is, a different NBR threshold was established for each of the 16 subimages.

Within each of the 16 subimages, the NBR threshold was determined based on the analysis of the best spatial correlation between burned area (as derived from each of the NBR subimages) and active fire influence area (as derived from the active fire locations). Thus, for each of the 16 subimages, we produced 21 different burned area maps (burned–unburned binary datasets) as a result of thresholding each NBR subimage using values ranging from −0.10 to 0.10 at intervals of 0.01 (NBR greater than or equal to −0.10, −0.09, −0.08, −0.07, −0.06, −0.05, −0.04, −0.03, −0.02, −0.01, 0.00, 0.01, 0.02, 0.03, 0.04, 0.05, 0.06, 0.07, 0.08, 0.09, and 0.10). For the MODIS active fire point format dataset, we first converted it into a binary image of 1-km pixel size, which is the spatial resolution of the MODIS active fire product, and we called the result the active fire influence area image. This image was then divided into the corresponding 16 subimages of 300 km by 300 km so as to cross tabulate them with the burned area subimages. At this point, it is worth pointing out that we only accounted for active fire locations with a confidence value higher than 60 and that occurred between 1 January and 2 February 2004.

The two sets of binary data (burned area and active fire influence area subimages) were then cross tabulated to find the NBR threshold value that best spatially correlated both sets of data. This way of finding the NBR threshold value ensured the greatest consistency between datasets, thus simultaneously accounting for both the burned area (according to the NBR criterion, which summarizes data from the NIR and SWIR parts of the spectrum) and the active fire influence area (which summarizes data from the middle- and thermal-infrared parts of the spectrum). The results of the cross tabulation between datasets were summarized in confusion matrices that were used to extract three parameters: (i) the overall accuracy, (ii) the kappa coefficient, and (iii) the omission and commission errors for the burned class.

Confusion matrices are frequently used to display information in a way that allows the assessment of the thematic accuracy of a land-cover map (Stehman 1996). Ideally, the confusion matrices should be reported whenever feasible (Stehman 1996). Otherwise, various accuracy measures that have been proposed will be of interest for summarizing the information content of a confusion matrix, with no single measure being universally accepted as the best option (Stehman 1996). Whenever the map accuracy measures are used during the process of creating a map, as was done in this work, such parameters should have the ability to rank the maps and measure the magnitude of their differences in accuracy (Stehman 1996). Considering all of the aspects reviewed, we decided to gather three parameters (overall accuracy, kappa coefficient, and omission and commission errors for the burned class) that were used to find an appropriate NBR threshold value for each of the 16 subimages. This set of 16 threshold values was properly applied to each subimage, resulting in 16 burned area maps. By making a mosaic of these maps, we finally produced the burned area map, which was validated and then compared with the results of two global burned area products (L3JRC and MCD45A1).

Table 1. Burned area mapping: relative contribution of each of the analyzed subimages (percentage of area with valid reflectance data), number of active fires for the study period (1 Jan–2 Feb 2004), accuracy measures used in each case, NBR threshold value, and burned area.

	Percentage of area with valid reflectance data	No. of active fires	Accuracy measures			NBR threshold value	Burned area (km^2)
			Overall accuracy	Kappa coefficient	Omission–commission errors		
w11	31.9	33	✓			0.00	32
w12	51.4	4				0.00	18
w13	95.5	49	✓		✓	0.05	49
w14	85.8	47	✓	✓		0.02	939
w21	1.7	0				0.00	0
w22	54.9	18	✓	✓	✓	0.00	40
w23	98.0	64	✓			0.08	67
w24	99.6	509	✓	✓		0.06	882
w31	1.0	0				0.00	0
w32	63.5	42	✓			0.03	45
w33	97.5	440	✓	✓	✓	0.01	442
w34	100.0	1867	✓	✓	✓	0.06	2376
w41	23.7	12	✓			0.07	13
w42	84.6	278	✓			0.00	5
w43	99.2	1267	✓			0.00	32
w44	100.0	212	✓			0.00	0
Total	68.0	4842	—	—	—	—	4940

The validation process served to verify the quality of the MODIS-based burned area map. The validation data (or ground truth) represent the reality (e.g., free from errors), and thus they serve as a reference to measure the accuracy of the classification process (Boschetti et al. 2004b). One of the most common means of validation in remote sensing is using data derived from higher-spatial-resolution images. In this case, we processed a Landsat-7 ETM+ image that partially covered the study area to produce a high-spatial-resolution burned area map (reference map). The processing of the Landsat-7 ETM+ image consisted of a supervised classification, followed by a visual interpretation and a manual editing of the burned polygons. In a second step, we compared the MODIS-based burned area map with this reference map by means of cross tabulation, the results of which were synthesized in an error matrix (Stehman 1996; Boschetti et al. 2004b).

As an element of this comparison, we also calculated the confusion matrices between our MODIS-based burned area map and two global burned area products (L3JRC and MCD45A1) in the same area and period.

4. Results

For each of the 16 analyzed subimages (Figure 1), Table 1 summarizes some of the key parameters that were involved in the MODIS-based burn mapping: for example, the number of active fires or the NBR threshold value. Table 1 also shows the burned area of each of the 16 subimages, as well as total burned area for the study area and period of interest, which indicated a total area of 4940 km^2.

During the MODIS-based burned area map development, we initially wondered about the availability of enough suitable reflectance samples (valid pixel values) within each of the 16 subimages. If the number of valid pixels or samples was not high enough, the spatial correlation analysis would have not been reliable, as occurs in subimages w21 (1.7%) and w31 (1.0%). In these two cases, we did not investigate the best NBR threshold value but set it to 0.00, which is the generally accepted burned–unburned threshold value (Key and Benson 1999). Thus, another important aspect of our investigation was to account for a high enough number of active fires within each subimage; otherwise, the NBR threshold could not be estimated using the proposed methodology. Whenever the number of active fires was too low, as occurs in subimage w12 (four active fires), the NBR threshold value was set to 0.00. For the remaining subimages (13 out of 16), we proceeded to analyze the three accuracy measures that we derived from the confusion matrices (Table 1). At this point, it is worth pointing out that such accuracy measures were used for ranking the NBR threshold values, rather than for assessing the accuracy of any final map (Stehman 1996).

As shown in Table 1, the overall accuracy was used in all the cases, while the other two accuracy measures were used occasionally. The interpretation of these parameters was as follows: on the one hand, for the overall accuracy and kappa coefficient, the higher they are, the better; on the other hand, the omission and commission errors behave as opposites, so the optimal value was set at the point where they crossed (as shown in Figure 3) in an attempt to find a trade-off between errors. Figure 3 shows two of these parameters for subimage w34. In this case, the two shown parameters revealed that an NBR threshold value of 0.00 or 0.01 was the one that produced the best results.

Figure 4 shows a detail (corresponding to subimage w34) of the NBR image, together with overlaying active fire locations (red dots) and the resulting burned area map for the 2004 fire season up until 1 February. The image on the left-hand side (Figure 4) shows the spatial agreement between the active fire locations (1867, shown in red dots) and postfire reflectance signal (high values of NBR, shown in white in this example), on which the methodology used in this report is based. Unfortunately, such spatial coherence was not found in all of the analyzed subimages. For example, in subimage w14, we detected 939 km^2 of burned area, whereas the number of active fires for the study period at this location was only 47. By contrast in subimage w43, the algorithm only detected 32 km^2 of burned area, whereas the total active fire locations during the study period reached the number of 1267.

The process of validating our results was conducted in the area shown in subimage w34, where most of the fires were concentrated. This subimage was partially covered by the Landsat-7 ETM+, as shown in Figure 5. The Landsat-7 ETM+ image was classified using a supervised classification algorithm, and the result was visually analyzed and manually edited. The resulting image was converted into vector format and compared, via cross tabulation, with the MODIS-based burned area map, which had also previously been converted into vector format. Table 2 summarizes the results. The overall accuracy was 95.47%, which was not particularly revealing, because it was mainly due to the large amount of unburned area that was rightly assigned to its category. The kappa coefficient, which measures the accuracy of the burn mapping process in eliminating potential random effects, was

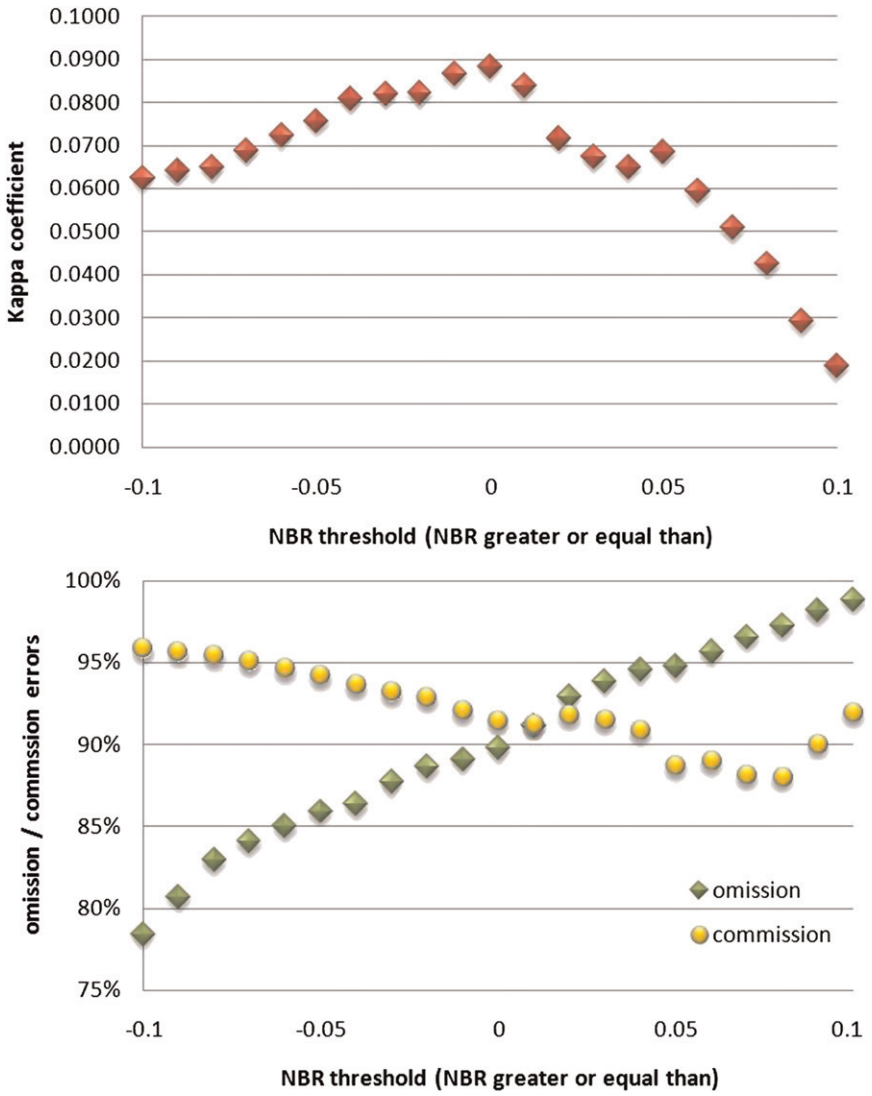

Figure 3. For subimage w34: (top) variation of the kappa coefficient and (bottom) omission and commission errors according to the different values of NBR.

0.56. Finally, the commission error for the burned category was 35.85%, and the omission error was 46.00%.

As an element of comparison, the resulting MODIS-based burned area map was compared to two global burned area products: L3JRC and MCD45A1. Within tile H10V08, the total affected area was 4940 km^2, which made for a valid area (land pixels with data) of 979 591 km^2. The overall accuracy of our product when compared to the L3JRC and MCD45A1 products was 92.52% and 97.14%, respectively. The burned area within the compared area was shown to be 4940 km^2 (our estimation), then 5461 km^2 (by the L3JRC), and then 2481 km^2 (by the MCD45A1). Figure 6 shows an example of this.

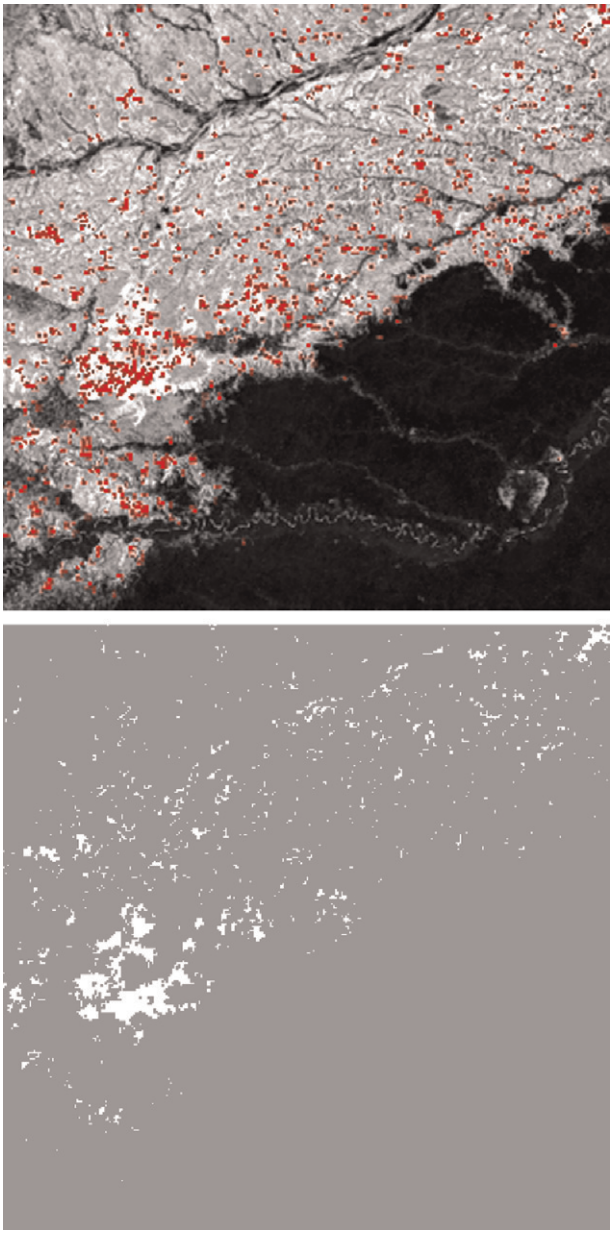

Figure 4. Subimage w34: (top) NBR with 1867 active fires (red dots) superimposed and (bottom) burned area map (NBR $\geq$ 0.06; 2376 km^2).

5. Discussion

The initial objective of performing a first test of a semiautomatic method for burn mapping in Latin America has been achieved. The approach is straightforward, easily implementable, and repeatable. However, further work is needed to improve the technique and to validate and compare its results using other regional or global satellite-based burned area products.

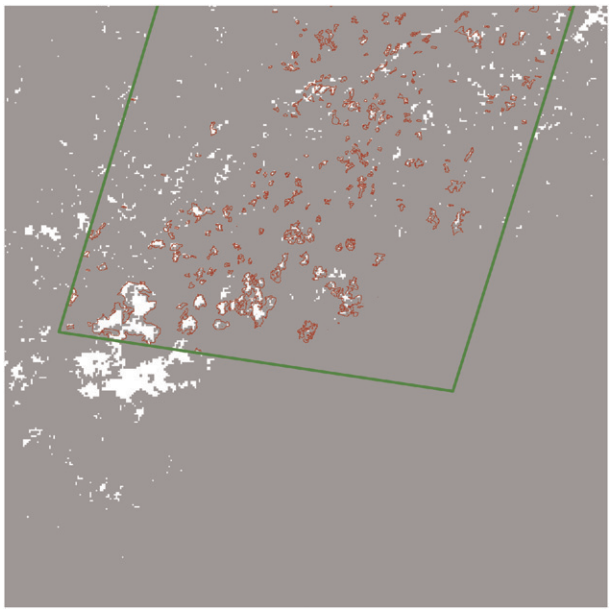

Figure 5. Subimage w34: MODIS-based burned area map (white patches; NBR $\geq$ 0.06; 2376 km^2) and reference map (delineated in dark red; Landsat scene limits shown in green).

According to our validation results, the algorithm developed in this study performed reasonably well within large, individually burned patches (patches over 1 km^2), which is the actual MODIS pixel size of the MCD43B4 product. The geographic accuracy for smaller fire scars was very low, which is partially explained by the coarse resolution of the MODIS images but is also due to the mild severity of many of the burned areas, such as those concentrated in the savannas (subimage 34). Other differences between datasets may be due to the dates when the MCD43B4 product and the Landsat-7 ETM+ images were obtained, which differ slightly.

Some of the difficulties that we encountered in mapping burned areas may be related to the input data, particularly for the MCD43B4 image, which is a 16-day product. The aim of using multitemporal composites in burn mapping is to solve some of the problems that can be found in daily images, such as cloud cover, cloud shadows, and off-nadir viewing (Van Leeuwen et al. 1999). However, daily images

Table 2. Error matrix for subimage w34.

		Reference map (km^2)				
		Unburned	Burned	Total	User's accuracy	Commission error
MODIS-based burned area map (km^2)	Unburned	29 012.96	859.70	29 872.66	97.12%	2.88%
	Burned	563.97	1009.27	1573.24	64.15%	35.85%
	Total	29 576.93	1868.97	31 445.90		
	Producer's accuracy	98.09%	54.00%			
	Commission error	1.91%	46.00%			

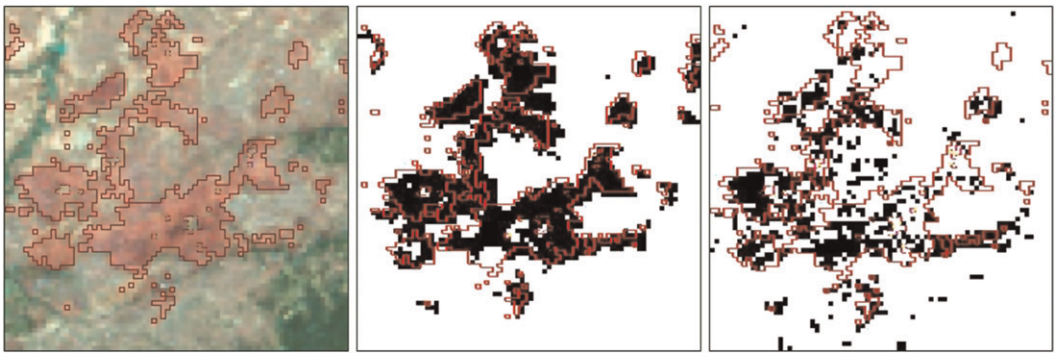

Figure 6. Subimage w34: (left) our estimation (delineated in red), (middle) L3JRC (in black), and (right) MCD45A1 (in black).

maintain radiometric changes more clearly than composites do, and fire scar mapping, particularly as related to the methodology used in this case, is a task that clearly benefits from larger differences. Unfortunately, there has not been much work done on burn mapping using MCD43B4 products, and it is therefore difficult to evaluate to what extent the use of this product may improve the results.

Finally, the comparison of our method with the two standard products (L3JRC and MCD45A1) produced interesting results. Our results confirm the known fact that the MODIS burned area product tends to underestimate burned areas (Roy et al. 2008; Giglio et al. 2009). By contrast, we found very close results, both in terms of total area and in terms of geographic accuracy, between our product and the L3JRC.

6. Concluding remarks

This article presents a methodology for burn assessment and mapping at a regional scale in a manner that could be easily expanded to global scales and therefore integrated into global change and climatic models. In particular, the methodology is applied here to the analysis of the effects of fires in Colombia during part of the 2004 fire season. It begins by presenting a semiautomatic algorithm for burned area mapping that uses remote sensing techniques and data and that was applied to the fires of a specific time in Colombia. Our second step was to validate results and compare them to two global burned area products (L3JRC and MCD45A1). Initially, we used MODIS satellite information from four different parts of the spectrum (NIR, SWIR, middle infrared, and thermal infrared). We developed a methodology based on the combination of a spectral index with active fire locations, which built on previous research (Roy et al. 1999; Fraser et al. 2000; Al-Rawi et al. 2001; Pu et al. 2004; Huesca et al. 2008; González-Alonso and Merino-de-Miguel 2009; Merino-de-Miguel et al. 2010) but also introduced innovations, like the use of the NBR index and MCD43B4 data. The overall result is a close approximation to actual burn boundaries within the limits of the MODIS pixel size.

This methodology produced reliable results largely because of its use of the best correlation between two sets of data, both of which come from a different part of

the spectrum. On the one hand, the NBR index is estimated using information from the NIR and SWIR channels, where reflective processes are dominant. On the other hand, active fire data are elaborated using information from the emissive part of the spectrum, where the MIR and TIR channels are located. However, it is important to note that, as burn mapping is obtained from the intersection of these two sets of data, the results will need to be adjusted to compensate for both commission and omission errors.

Acknowledgments. The authors thank NASA/University of Maryland for providing us with the *Terra*/*Aqua* MODIS active fire products; Global Land Cover Facility/University of Maryland for providing us with the Landsat-EMT+ image; EOS Data Gateway for providing us with the MCD43B4 and MCD45A1 products; and finally the Joint Research Center (JRC) for providing us with the L3JRC product. This research was possible thanks to the supporting project A/016220/08 from the PCI-IBEROAMERICA Program [Agencia Española de Cooperación Internacional para el Desarrollo (AECID)]. The anonymous reviewers are also thanked for their comments.

References

Al-Rawi, K. R., J. L. Casanova, and A. Romo, 2001: IFEMS: A new approach for monitoring wildfire evolution with NOAA-AVHRR imagery. *Int. J. Remote Sens.,* **22,** 2033–2042.

Armenteras, D., M. Romero, and G. Galindo, 2005: Vegetation fire in the savannas of the Llanos Orientales of Colombia. *World Resour. Rev.,* **17,** 531–543.

——, F. González-Alonso, and C. Franco, 2009: Distribución espacial y temporal de incendios en Colombia utilizando datos de anomalías térmicas. *Caldasia,* **31,** 291–306.

Boschetti, L., H. D. Eva, P. A. Brivio, and J. M. Grégoire, 2004a: Lessons to be learned from the comparison of three satellite-derived biomass burning products. *Geophys. Res. Lett.,* **31,** L21501, doi:10.1029/2004GL021229.

——, E. P. Flasse, and P. A. Brivio, 2004b: Analysis of the conflict between omission and commission in low spatial resolution dichotomic thematic producers: The Pareto Boundary. *Remote Sens. Environ.,* **91,** 280–292.

Chang, D., and Y. Song, 2009: Comparison of L3JRC and MODIS global burned area products from 2000 to 2007. *J. Geophys. Res.,* **114,** D16106, doi:10.1029/2008JD011361.

Chuvieco, E., and Coauthors, 2008: Global burned-land estimation in Latin America using MODIS composite data. *Ecol. Appl.,* **18,** 64–79.

Cochrane, M. A., and W. F. Laurance, 2008: Synergisms among fire, land use, and climate change in the Amazon. *Ambio,* **37** (7-8), 522–527.

Fraser, R. H., Z. Li, and J. Cihlar, 2000: Hotspot and NDVI Differencing Synergy (HANDS): A new technique of burned area mapping over boreal forest. *Remote Sens. Environ.,* **74,** 362–376.

Friedl, M. A., D. Muchoney, D. McIver, F. Gao, J. F. C. Hodges, and A. H. Strahler, 2000: Characterization of North American land cover from NOAA-AVHRR data using the EOS MODIS land cover classification algorithm. *Geophys. Res. Lett.,* **27,** 977–980.

Giglio, L., J. Descloitres, C. O. Justice, and Y. J. Kaufman, 2003: An Enhanced Contextual Fire Detection Algorithm for MODIS. *Remote Sens. Environ.,* **87,** 273–282.

——, I. Csiszar, and C. O. Justice, 2006a: Global distribution and seasonality of active fires as observed with the Terra and Aqua Moderate Resolution Imaging Spectroradiometer (MODIS) sensors. *J. Geophys. Res.,* **111,** G02016, doi:10.1029/2005JG000142.

——, G. R. van der Werf, J. T. Randersron, G. J. Collatz, and P. Kasibhatla, 2006b: Global estimation of burned area using MODIS active fire observations. *Atmos. Chem. Phys.,* **6,** 957–974.

——, T. Lodoba, D. P. Roy, B. Quayle, and C. O. Justice, 2009: An active-fire based burned area mapping algorithm for the MODIS sensor. *Remote Sens. Environ.,* **113,** 408–420.

González-Alonso, F., and S. Merino-de-Miguel, 2009: Integration of AWiFS and MODIS active fire data for burn mapping at regional level using the Burned Area Synergic Algorithm (BASA). *Int. J. Wildland Fire,* **18,** 404–414.

Grégoire, J. M., K. Tansey, and J. M. M. Silva, 2003: The GBA initiative: Developing a global burned area database from SPOT-VEGETATION imagery. *Int. J. Remote Sens.,* **24,** 1369–1376.

Hoffmann, W. A., B. Orthen, and P. K. Vargas Do Nascimento, 2003: Comparative fire ecology of tropical savanna and forest trees. *Funct. Ecol.,* **17,** 720–726.

Huesca, M., F. González-Alonso, J. M. Cuevas, and S. Merino-de-Miguel, 2008: Estimación de la superficie quemada en los incendios forestales de Canarias de 2007 utilizando sinérgicamente imágenes MODIS y anomalías térmicas. *Inves. Agrar. Sistemas Recur. For.,* **17,** 308–316.

Justice, C. O., and Coauthors, 2002: The MODIS fire products. *Remote Sens. Environ.,* **83,** 244–262.

Kerr, J. K., and M. Ostrovsky, 2003: From space to species: Ecological applications for remote sensing. *Trends Ecol. Evol.,* **18,** 299–305.

Key, C. H., and N. C. Benson, 1999: Measuring and remote sensing of burn severity: The CBI and NBR. *Proc. Joint Fire Science Conf. and Workshop,* Boise, ID, University of Idaho and International Association of Wildland Fire, [Available online at http://www.nrmsc.usgs.gov/files/norock/products/SEVER36_im_copy6.pdf.]

Lentile, L. B., and Coauthors, 2006: Remote sensing techniques to assess active fire characteristics and post-fire effects. *Int. J. Wildland Fire,* **15,** 319–345.

Loboda, T., K. J. O'Neal, and I. Csiszar, 2007: Regionally adaptable dNBR-based algorithm for burned area mapping from MODIS data. *Remote Sens. Environ.,* **109,** 429–442.

Merino-de-Miguel, S., M. Huesca, and F. González-Alonso, 2010: MODIS reflectance and active fire data for burn mapping and assessment at regional level. *Ecol. Modell.,* **221,** 67–74.

NASA Landsat Program, 2004: Landsat ETM+ scene L71006057_05720040201, SLC_Off. USGS. [Available online at http://glcf.umiacs.umd.edu/data/landsat/.]

NASA/University of Maryland, 2002: MODIS hotspot/active fire detections. MODIS Rapid Response Project, NASA/GSFC, University of Maryland, Fire Information for Resource Management System Dataset. [Available online at http://maps.geog.umd.edu.]

Pozo, D., F. J. Olmo, and L. Alados Arboledas, 1997: Fire detection and growth monitoring using a multi-temporal technique on AVHRR mid-infrared and thermal channels. *Remote Sens. Environ.,* **60,** 111–120.

Pu, R., P. Gong, Z. Li, and J. Scarborough, 2004: A dynamic algorithm for wildfire mapping with NOAA/AVHRR data. *Int. J. Wildland Fire,* **13,** 275–285.

Roldán-Zamarrón, A., S. Merino-de-Miguel, F. González-Alonso, S. García-Gigorro, and J. M. Cuevas, 2006: Minas de Riotinto (south Spain) forest fire: Burned area assessment and fire severity mapping using Landsat 5-TM, Envisat-MERIS, and Terra-MODIS postfire images. *J. Geophys. Res.,* **111,** G04S11, doi:10.1029/2005JG000136.

Roy, D. P., L. Giglio, J. D. Kendall, and C. O. Justice, 1999: Multi-temporal active-fire based burn scar detection algorithm. *Int. J. Remote Sens.,* **20,** 1031–1038.

——, P. E. Lewis, and C. O. Justice, 2002: Burned area mapping using multi-temporal moderate spatial resolution data—A bi-directional reflectance model-based expectation approach. *Remote Sens. Environ.,* **83,** 263–286.

——, Y. Jin, P. E. Lewis, and C. O. Justice, 2005: Prototyping a global algorithm for systematic fire-affected area mapping using MODIS time series data. *Remote Sens. Environ.,* **97,** 137–162.

——, L. Boschetti, C. O. Justice, and J. Ju, 2008: The collection 5 MODIS burned area product—Global evaluation by comparison with the MODIS active fire product. *Remote Sens. Environ.,* **112,** 3690–3707.

Schaaf, C., cited 2010: MODIS BRDF/albedo product (MOD43B) user's guide. MODIS. [Available online at http://www-modis.bu.edu/brdf/userguide/nbar.html.]

——, and Coauthors, 2002: First operational BRDF, albedo and nadir reflectance products from MODIS. *Remote Sens. Environ.,* **83,** 135–148.

Simon, M., S. Plummer, F. Fierens, J. J. Hoelzemann, and O. Arino, 2004: Burnt area detection at global scale using ATSR-2: The GLOBSCAR products and their qualification. *J. Geophys. Res.,* **109,** D14S02, doi:10.1029/2003JD003622.

Stehman, S. V., 1996: Selecting and interpreting measures of thematic classification accuracy. *Remote Sens. Environ.,* **62,** 77–89.

Tansey, K., and Coauthors, 2004: Vegetation burning in the year 2000: Global burned area estimates from SPOT VEGETATION data. *J. Geophys. Res.,* **109,** D14S03, doi:10.1029/2003JD003598.

——, J. M. Grégoire, P. Defourny, R. Leigh, J. F. Pekel, E. van Bogaert, and E. Bartholomé, 2008: A new, global, multi-annual (2000-2007) burnt area product at 1 km resolution. *Geophys. Res. Lett.,* **35,** L01401, doi:10.1029/2007GL031567.

Van der Werf, G. R., J. T. Randerson, L. Giglio, G. J. Collatz, P. S. Kasibhatla, and A. F. Arellano Jr., 2006: Interannual variability of global biomass burning emissions from 1997 to 2004. *Atmos. Chem. Phys.,* **6,** 3423–3441.

Van Leeuwen, W. J. C., A. R. Huete, and T. W. Laing, 1999: MODIS vegetation index compositing approach: A prototype with AVHRR data. *Remote Sens. Environ.,* **69,** 264–280.